16th Australasian Fluid Mechanics Conference
Crown Plaza, Gold Coast, Australia
2-7 December 2007

Comparative Assessment of LES and URANS for Flow Over a Cylinder at a Reynolds Number of 3900

M. E. Young[1] **and A. Ooi**[2]

[1]Flight Systems, Air Vehicles Division
Defence Science and Technology Organisation, Fishermans Bend, 3207 AUSTRALIA

[2]Department of Mechanical and Manufacturing Engineering
University of Melbourne, Melbourne, 3010 AUSTRALIA

Abstract

Numerical simulations utilising turbulence models based on the Reynolds Averaged Navier Stokes (RANS) equations generally exhibit poor performance in predicting separated flow around cylinders. This paper assesses potential improvements offered by the three-dimensional unsteady RANS and Large Eddy Simulation (LES) methodologies in replicating the flow around a cylinder at a Reynolds number, based on diameter, of 3900. The performance is assessed against corresponding experimental data and two-dimensional unsteady RANS turbulence simulations.

Introduction

This paper presents a comparison of two computational fluid dynamics (CFD) techniques in modelling the flow over a circular cylinder in crossflow at a Reynolds number based on cylinder diameter of 3900. RANS models have formed the basis for CFD analysis of engineering flows for many years, the unsteady Reynolds-Averaged Navier-Stokes (URANS) models are an extension of RANS where the time-dependent terms are included in the governing equations. RANS and URANS methods model turbulence through additional differential equations approximating the effects of turbulence length and time scales, whilst large-eddy simulation (LES) resolves eddies that are larger than the grid size and models the subgrid scale effects using an algebraic model. URANS calculations are feasible on even modest computational facilities, whereas LES usually requires substantial computing power even at relatively low Reynolds numbers.

The flow around a cylinder is often used as a test case for CFD codes as it offers a simple geometry that gives rise to inherently complex flow phenomena. The Reynolds number dictates the nature of the flow, and several distinct regimes have been identified. As was found by Roshko [16], at Reynolds numbers below 40 the entire flow is laminar, steady and symmetrical; in the stable range between 40 and 150 the flow is entirely laminar and a regular and stable vortex street exists; the transition range is from 150 to 300 where there is laminar to turbulent transition in the shear layer; and above 300 is the irregular range, which exhibits a Strouhal number that is relatively independent of Reynolds number. Mittal and Balachandar [11] note that the flow transitions from two- to three-dimensional at a Reynolds number of approximately 180. At much higher Reynolds numbers (2×10^5 to 5×10^5) laminar separation is immediately followed by transition to turbulence and subsequent reattachment of the flow on the downstream side of the cylinder followed by separation of the turbulent boundary layer. This regime is characterised by a reduction in the width of the wake, a commensurate reduction in drag coefficient, and an increase in the Strouhal number. From 5×10^5 to 3.5×10^6 the transition to turbulence occurs in the boundary layer prior to separation and the wake is fully turbulent [17]. It is worth noting that the exact Reynolds numbers defining the boundaries between the different regimes are sensitive to various experimental parameters such as freestream turbulence [12], cylinder end conditions [20] and other influences, and so may differ from experiment to experiment.

The present study, at a Reynolds number of 3900, falls into Roshko's irregular range. We can therefore expect a laminar separation followed by a transition to turbulence in the separated shear layer, and a three-dimensional turbulent wake. The selection of this Reynolds number was dictated both by its tractability using large-eddy simulation (LES) on available computational facilities, and the availability of a comprehensive range of experimental data available for comparison. Not surprisingly, several other studies have investigated LES at the same Reynolds number, including [1], [2], and [8]. These papers serve to illustrate the development of LES over recent years, including the evolution of numerical schemes and subgrid scale models.

Of the methods available to model this flow, steady RANS models are obviously unsuitable due to the inherent unsteadiness at this Reynolds number. Two-dimensional URANS has also been shown, for example in [5], to be inaccurate with overprediction of the drag and base pressure coefficients, a shorter recirculation region aft of the cylinder, and stronger vortices shed in the wake. Therefore, much has been written (see [11] and [18]) on the importance of the spanwise dimension at Reynolds numbers where the flow is three-dimensional. This study assesses how well a three-dimensional URANS calculation compares to LES simulations and the sensitivity of the data to various levels of spanwise resolution.

Computational Details

The computational domain is presented in figure 1. The domain extended 15D forward, above and below the cylinder and 25D aft of the cylinder where D denotes cylinder diameter. The spanwise domain (for the three-dimensional cases) was πD, which

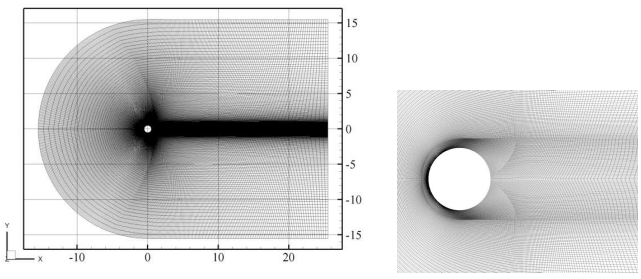

(a) (b)

Figure 1: (a) Mesh of the entire computational domain; (b) detail of mesh near cylinder.

Mesh	N_{total}	N_r	N_w	N_a	N_z
2D URANS	90×10^3	150	150	300	–
3D URANS	1.44×10^6	150	150	300	16
LES $n_z = 4$	360×10^3	150	150	300	4
LES $n_z = 16$	1.44×10^6	150	150	300	16
LES $n_z = 32$	2.88×10^6	150	150	300	32
LES $n_z = 48$	4.32×10^6	150	150	300	48

Table 1: Details of the computational grids used in the study (N_r denotes number of radial nodes; N_w denotes number of nodes in the wake; N_a denotes number of azimuthal nodes; and N_z denotes the number of spanwise elements).

Case	Run time (hrs)	CPUs	Total CPU Time (hrs)
2D URANS	17	1	17
3D URANS $n_z = 16$	450	1	450
LES $n_z = 4$	36	4	145
LES $n_z = 16$	233	4	930
LES $n_z = 32$	147	8	1171
LES $n_z = 48$	223	8	1784

Table 2: The computational time required for 30 shedding periods.

was consistent with numerous other computational studies (e.g. [1] and [8]). Details of the grid are presented in table 1. URANS simulations were performed using both a two-dimensional grid and a three-dimensional grid with 16 spanwise cells. LES cases were run with 4, 16, 32, and 48 spanwise cells. All cases used the same two-dimensional cross-section seen in figure 1.

The LES solutions were performed using an unstructured finite volume code for incompressible flow, which employs a non-dissipative and energy conserving numerical method, details of which can be found in references [6] and [10]. The dynamic Smagorinsky sub-grid scale model was chosen over the standard (constant coefficient) Smagorinsky model based on other studies, for example [8], where the dynamic model was shown to be superior. The URANS solutions were carried out on a different unstructured finite volume code for incompressible flow, for which details are given in [4]. The standard k-ω two-equation turbulence model [19] was used.

The simulation was executed until the start-up transients had been convected through the domain and the flow had evolved to steady shedding before any statistics or flow properties were recorded, refer to figure 2. In the case of the LES simulations, this was approximately 60 non-dimensional units of flow time (tD/U_∞). The LES simulations were advanced through time with a CFL (Courant) number of one, which resulted in a timestep of approximately 4×10^{-3}. The URANS cases used a timestep of 0.05; a discussion on this matter is included in the following section. Table 2 presents the computational time required to simulate 30 shedding periods for each of the models and grids. Not surprisingly the computational requirements of the two-dimensional URANS case was by far the smallest, requiring less than a day on a single processor. At the other extreme was the 48 spanwise cell LES case, which used 8 CPUs for almost ten days in order to simulate the equivalent flow time. Whilst differences in numerics and convergence criteria make a direct comparison between the two methods difficult, the two cases with $n_z = 16$ show that the URANS case requires less computational time. This was in part because the timestep for the URANS simulation is an order of magnitude larger than in the LES simulation.

Case	$\overline{C_D}$	$\overline{C_{p_b}}$	St	$C_{L_{rms}}$
Experiment [3], [12], [13]	0.98 $\pm$ 0.05	0.90 $\pm$0.005	0.215 $\pm$0.005	0.03 – 0.08
2D URANS	1.59	1.96	0.235	1.17
3D URANS	1.32	1.42	0.223	0.701
LES $n_z = 4$	1.55	1.86	0.217	1.08
LES $n_z = 16$	1.25	1.36	0.196	0.549
LES $n_z = 32$	1.04	0.913	0.212	0.164
LES $n_z = 48$	1.03	0.908	0.212	0.177
[8]	1.04	0.94	0.210	n/a

Table 3: Overall flow parameters obtained over 30 shedding periods.

Results

The overall forces acting on the cylinder are important parameters for practical applications of CFD. Table 3 presents experimental data alongside the mean drag, $\overline{C_D}$, the mean base pressure coefficient, $\overline{C_{p_b}}$, Strouhal number, $St = nD/V$, and RMS of the lift coefficient, $C_{L_{rms}}$, for each of the CFD cases. Pressure drag arising from the wake downstream of the cylinder is the largest contribution to drag at this Reynolds number. The base pressure coefficient is a good indicator of whether the pressure in the wake is correct and therefore whether the overall drag will be correct. The Strouhal number is the non-dimensional frequency of the vortex shedding. The mean lift coefficient is ostensibly zero and therefore provides no insight into the flow; however, the RMS of the lift coefficient is included because it gives an indication of the strength and variability of the vortices being shed.

Clearly from table 3 the two-dimensional URANS predictions are very poor, considerably overestimating all the parameters. The four spanwise cell LES case shows very similar results to the two-dimensional URANS case for most of the parameters other than Strouhal number, which is slightly improved. Including the spanwise dimension in the URANS case results in only minor improvement. Note the 16 spanwise cell LES case offers similar results to the URANS case using the same grid. This suggests that LES is only effective when used with sufficient number of cells in the spanwise direction to resolve the smaller three-dimensional eddies. The improvement in the results for the higher spanwise resolution LES cases is impressive with the 48 cell case closely approximating the first three parameters. An additional comparison with a second LES study ([8]) is also provided and shows similar results to the current study.

Figure 2 presents the evolution of the lift and drag coefficients for the LES cases. A progressive reduction in amplitude of both lift and drag oscillations as the spanwise resolution increases from the quasi-two-dimensional cases (LES with four spanwise cells) through to the fully three-dimensional cases (LES with 32 and 48 spanwise cells) is evident. Also apparent is the reduction in drag coefficient as the three-dimensionality increases. Refer to figure 13 for the force coefficient time histories of the three-dimensional URANS case where the temporally resolved cases (i.e. $\Delta tD/U_\infty = 0.05$ and $\Delta tD/U_\infty = 0.025$) demonstrate behaviour similar to the LES case with 16 spanwise cells.

As suggested earlier, an accurate pressure distribution around the cylinder is critical for realistic prediction of forces on the cylinder. The pressure distribution around the cylinder is presented in figure 3 where it can be seen that the two- and quasi-

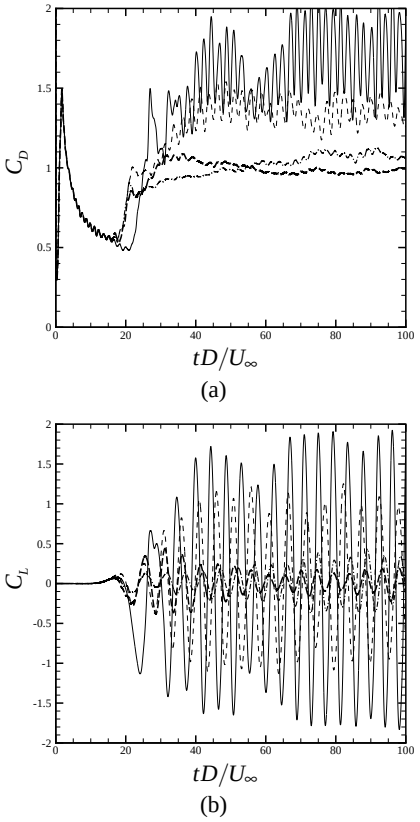

Figure 2: Time histories of (a) drag coefficient; and, (b) lift coefficient for LES on different meshes: ——— $n_z = 4$; – – – – $n_z = 16$; —·— $n_z = 32$; — — — $n_z = 48$.

two-dimensional cases all overestimate the pressure gradient on the front side of the cylinder, suggesting the three-dimensional influence is important even in the laminar flow prior to separation. The pressure distribution of the three-dimensional URANS case transitions between the four spanwise cell LES case on the forward half of the cylinder to the 16 spanwise cell LES case in the wake. The 32 and 48 spanwise cell cases overlay each other and are very close to the experimental data, as would be expected given the mean drag coefficient results from table 3. Again, the LES of [8] shows similar results.

The gross quantities such as drag and Strouhal number provide some insight into how well the models perform, but more information regarding the actual flow can be gained from comparison with the experimental studies of [9] and [14]. These provide a range of flow parameters, including mean and fluctuating streamwise and crossflow velocities, in the wake of the cylinder from $x/D = 0.58$ through to $x/D = 10$. Figure 4 presents the mean streamwise velocity along the centreline, aft of the cylinder. Both URANS cases, and the four and 16 cell LES cases underestimate the length of the recirculation region whilst the other LES cases and [8] overestimate the length. Figure 5 depicts the streamlines of the time-averaged flow, and illustrates the variation in the re-circulation length of the mean flow between the two models and the different resolutions. Reference [8] outlines some concerns regarding the results of [9], hypothesising that disturbances in the experiment triggered earlier transition and resulted in a shorter recirculation region, thereby explaining some of the discrepancies between the computational results (both the present study and [8]) and the experimental results of [9].

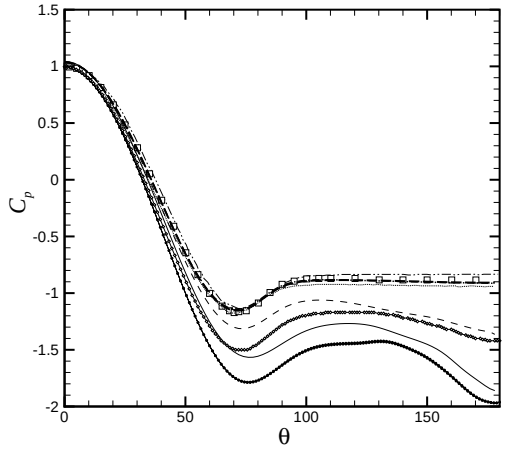

Figure 3: Comparison of the distribution of pressure coefficient around the cylinder: —··— [12] at $Re = 3000$; □ Norberg in [8] at $Re = 4020$; ——— $n_z = 4$; – – – – $n_z = 16$; —·— $n_z = 32$; — — — $n_z = 48$; ····· [8]; —●— $2D$ URANS; —◇— $3D$ URANS (at $\Delta tD/U_\infty = 0.05$).

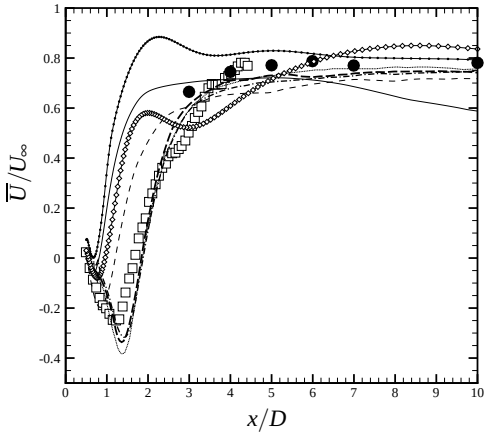

Figure 4: Mean streamwise velocity along the centreline aft of the cylinder: □ [9]; ● [14]; ——— $n_z = 4$; – – – – $n_z = 16$; —·— $n_z = 32$; — — — $n_z = 48$; ····· [8]; —●— $2D$ URANS; —◇— $3D$ URANS.

Figures 6 to 9 present the parameters at various downstream stations. The LES cases offer the closest comparison with the experimental data, and the results improve with spanwise resolution as expected. The 48 cell LES case offers only a marginal improvement over the 32 cell case. Very close to the cylinder at $x/D = 0.58$ all the models accurately estimate mean streamwise velocity. The URANS and coarse LES cases perform poorly beyond $x/D = 1.06$, whilst the fine LES cases perform well other than overpredicting the peak values on the centreline, which is consistent with the comparison of centreline velocity presented in figure 4. The mean crossflow velocities do not correspond very well with the experimental data from [9]; however, it is consistent with the LES data from [8] again raising concerns with the data from [9].

Both the streamwise and crossflow velocity fluctuations are well predicted from $x/D = 4$ to $x/D = 6$. At $x/D = 3$ they are both

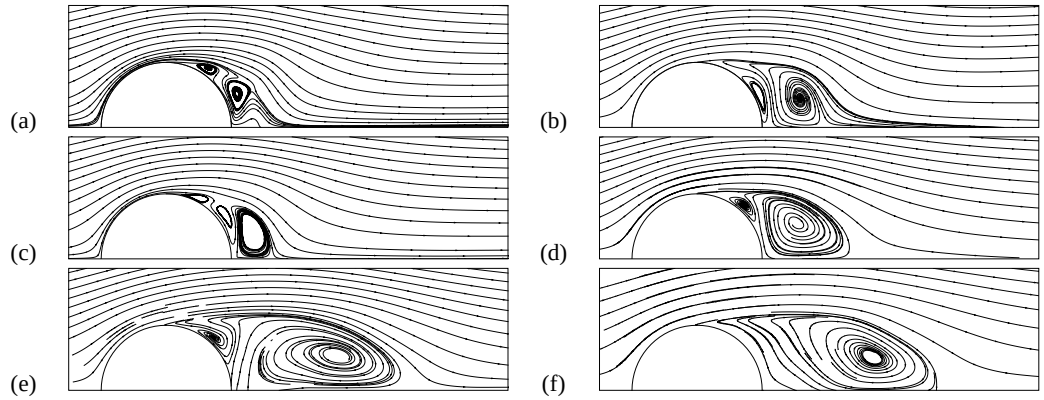

Figure 5: Streamlines of the time averaged flow for (a) 2D URANS; (b) 3D URANS with $n_z = 16$; (c) LES with $n_z = 4$; (d) LES with $n_z = 16$; (e) LES with $n_z = 32$; (f) LES with $n_z = 48$.

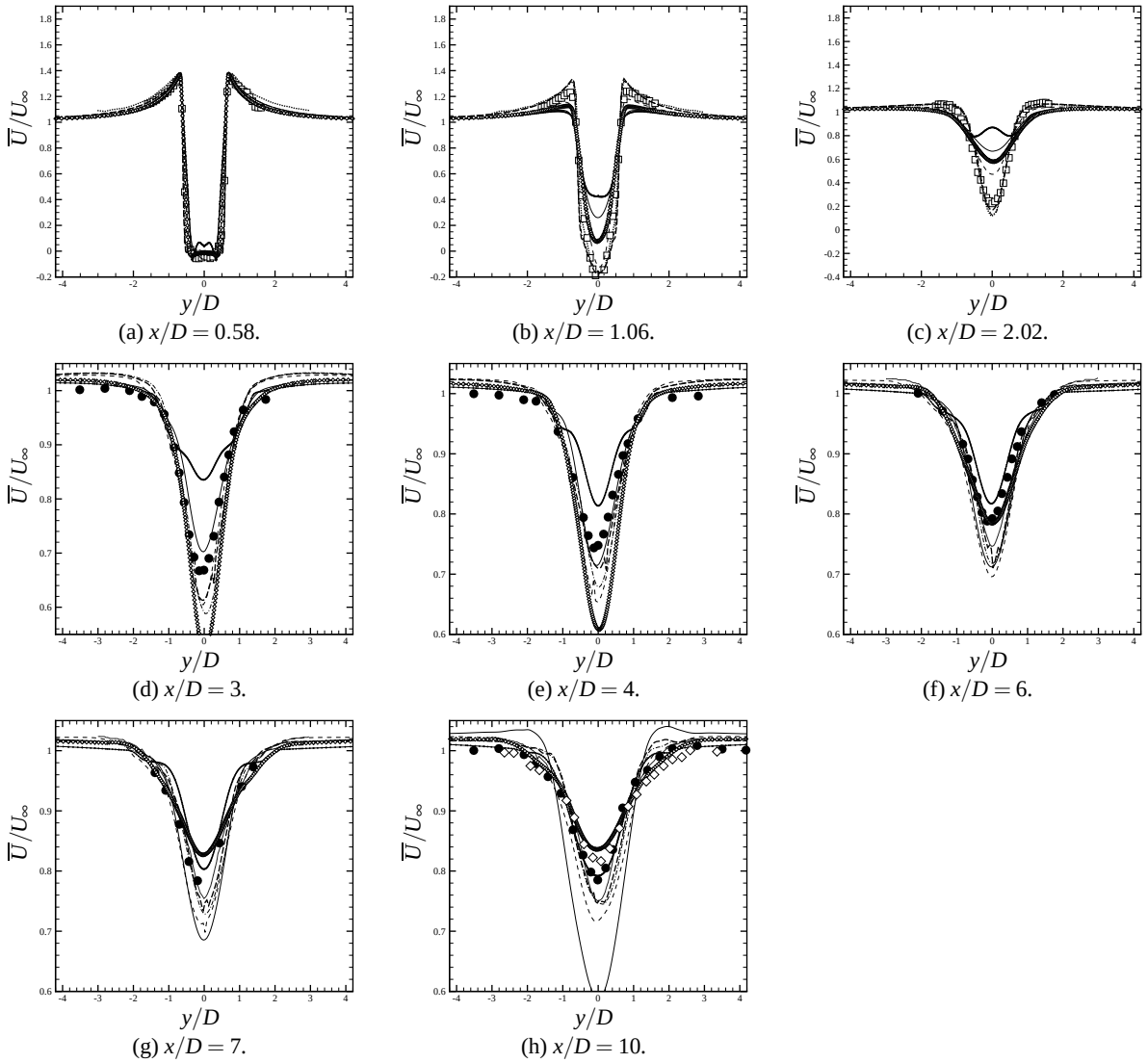

(a) $x/D = 0.58$. (b) $x/D = 1.06$. (c) $x/D = 2.02$.

(d) $x/D = 3$. (e) $x/D = 4$. (f) $x/D = 6$.

(g) $x/D = 7$. (h) $x/D = 10$.

Figure 6: Comparison of mean streamwise velocity. □ [9]; ● [14]; ◇ [21]; —— $n_z = 4$; - - - - $n_z = 16$; —·— $n_z = 32$; — — — $n_z = 48$; ····· [8]; —●— 2D URANS; —◇— 3D URANS.

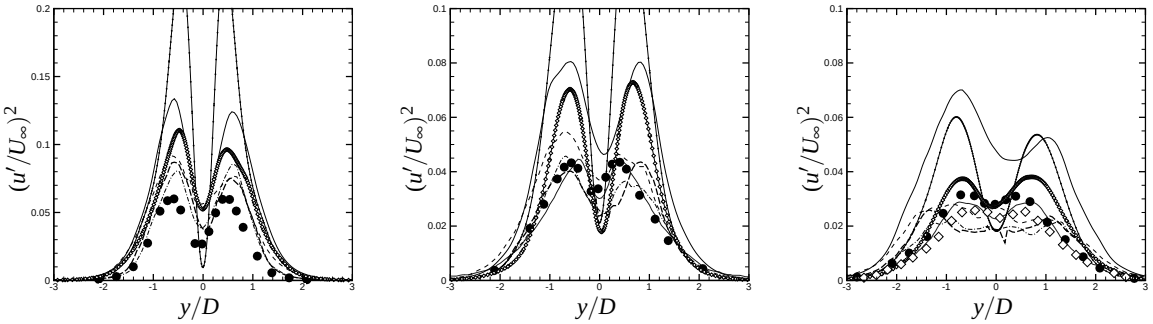

(a) $x/D = 3$. (b) $x/D = 6$. (c) $x/D = 10$.

Figure 7: Comparison of streamwise velocity fluctuations. ● [14]; ◇ [21]; —— $n_z = 4$; - - - - $n_z = 16$; —·— $n_z = 32$; — — — $n_z = 48$; ····· [8]; —●— 2D URANS; —◇— 3D URANS.

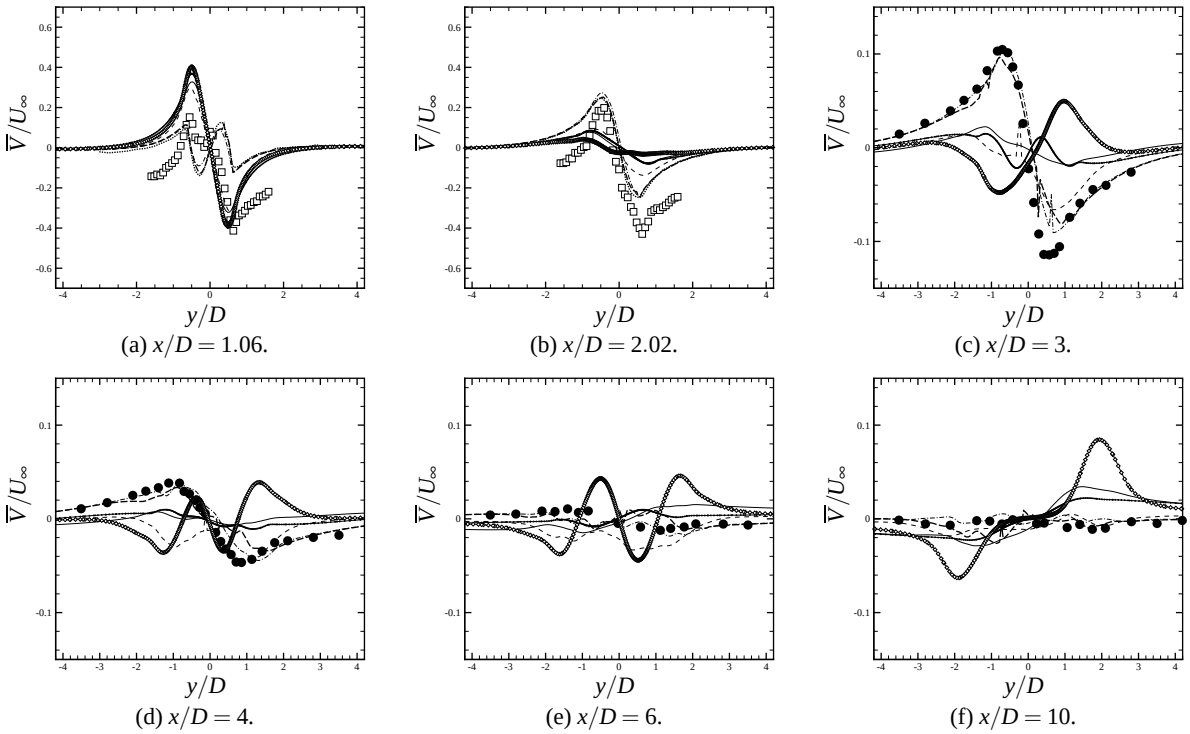

(a) $x/D = 1.06$. (b) $x/D = 2.02$. (c) $x/D = 3$.

(d) $x/D = 4$. (e) $x/D = 6$. (f) $x/D = 10$.

Figure 8: Comparison of mean crossflow velocity. □ [9]; ● [14]; —— $n_z = 4$; - - - - $n_z = 16$; —·— $n_z = 32$; — — — $n_z = 48$; ····· [8]; —●— 2D URANS; —◇— 3D URANS.

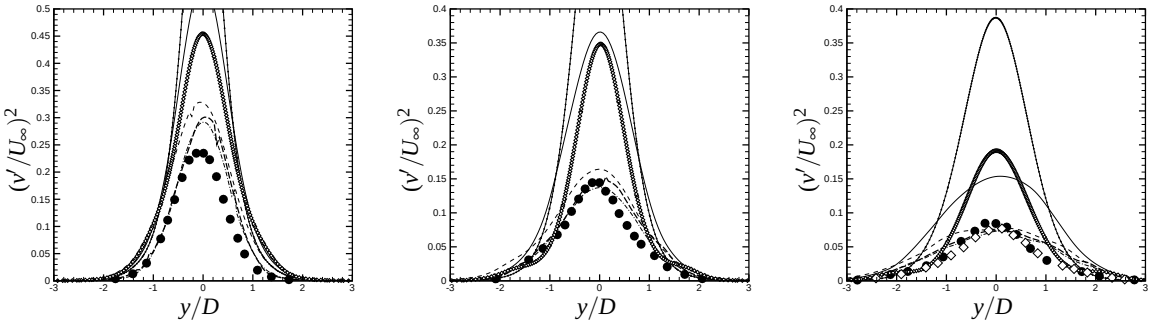

(a) $x/D = 3$. (d) $x/D = 6$. (f) $x/D = 10$.

Figure 9: Comparison of crossflow velocity fluctuations. ● [14]; ◇ [21]; —— $n_z = 4$; - - - - $n_z = 16$; —·— $n_z = 32$; — — — $n_z = 48$; ····· [8]; —●— 2D URANS; —◇— 3D URANS.

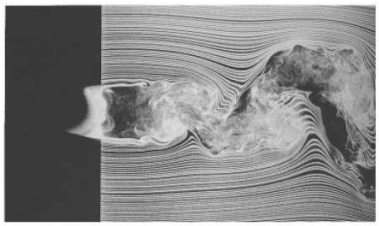

(a)

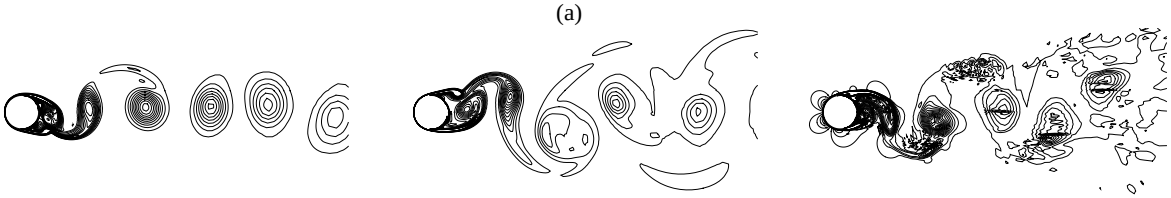

(b) 2D URANS. (c) 3D URANS with $n_z = 16$. (d) LES with $n_z = 4$.

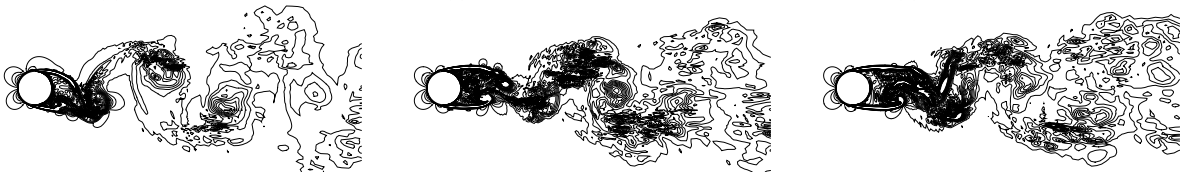

(e) LES with $n_z = 16$. (f) LES with $n_z = 32$. (g) LES with $n_z = 48$.

Figure 10: (a) Streaklines at $Re = 4000$ (from [15]). (b)–(g) Contours of vorticity magnitude at $Re = 3900$. There are 16 contour levels between 0.5 and 10.

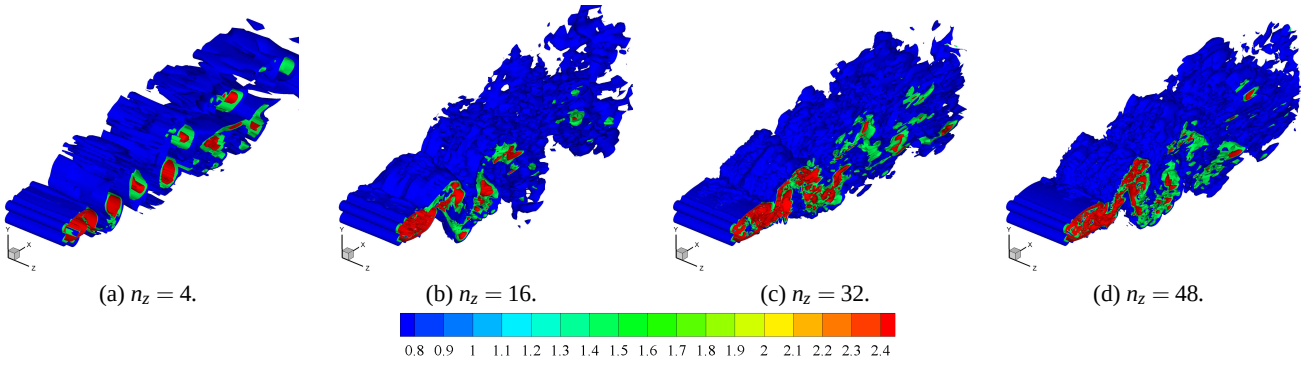

(a) $n_z = 4$. (b) $n_z = 16$. (c) $n_z = 32$. (d) $n_z = 48$.

Figure 11: Isosurfaces of vorticity magnitude for LES simulations with varying spanwise resolution.

overpredicted by all the models. Further downstream at $x/D = 7$ and $x/D = 10$ the present LES results for the streamwise fluctuations are slightly inferior to [8], possibly due to the coarseness of the stretched mesh downstream of the cylinder; however, the crossflow fluctuations match experimental data.

Figure 10(a) shows the streaklines about a cylinder at a Reynolds number of 4000 from [15]. The shear layer extends quite far downstream, which is a characteristic of the flow at this Reynolds number [8]. In comparison, figures 10(b) and (c) show the contours of vorticity magnitude for the two- and three-dimensional URANS cases, which demonstrate vortex roll up very close to the cylinder with very little shear layer development. Figures 10(d) to (g) show the appearance of smaller scales and the lengthening of the shear layer as spanwise resolution is increased in the LES cases. Similar results can be seen in [8]. Comparing figure 10(c) with (e) shows the difference between URANS and LES on the same mesh. Some smaller scales are evident in the latter, as is a reduction in the strength of the vorticity as the flow moves downstream; however, the flows are quite similar when assessed on a qualitative basis such as the vortex position and length of the shear layer.

Figure 11 presents isosurfaces of vorticity magnitude for each of the LES cases, revealing the degree of three-dimensionality in the flow for each. The flowfield in the four spanwise cell case in (a) is essentially two-dimensional, the 16 cell case in (b) shows some three dimensionality, although on a larger scale than the eddies exhibited by the 32 and 48 cell cases in (c) and (d) respectively. The latter case may also show some larger scale structures forming downstream of the shear layer, although it is not very clear. Figure 12(b) presents the three-dimensional URANS case, which also exhibits three-dimensional features with several streamwise vortices forming across the span and, although not apparent from the contour values used in the figure, hairpin vortices.

In developing the three-dimensional URANS case, the following observations regarding the timestep were made. This case was originally run with a non-dimensional timestep of 0.1 with the intention of flushing the transients from the domain, then

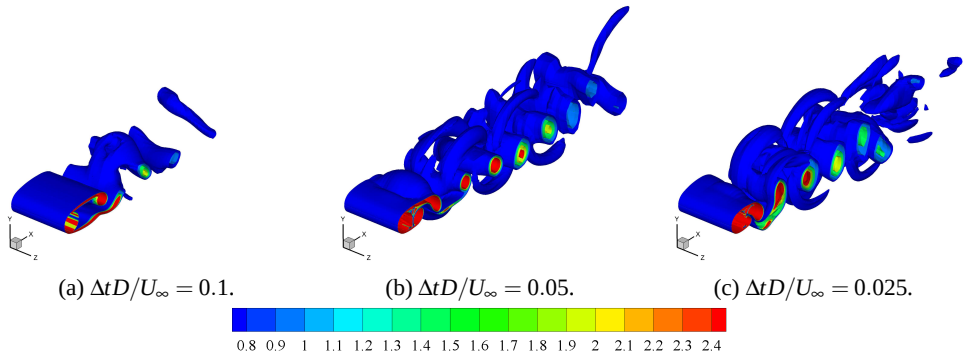

(a) $\Delta tD/U_\infty = 0.1$. (b) $\Delta tD/U_\infty = 0.05$. (c) $\Delta tD/U_\infty = 0.025$.

Figure 12: Isosurfaces of vorticity magnitude for three-dimensional URANS simulations with different timesteps.

switching to a finer timestep in order to record the flow statistics. Figure 13 shows the evolution of the lift and drag coefficients during this time. At a non-dimensional flow time of 69.7, the flowfield of which is presented in figure 14(a), the timestep was switched to 0.05, and the result was an immediate increase in drag coefficient and in the oscillation amplitude of the lift coefficient. This was accompanied by a change to the flowfield depicted in figure 14(b), which has much shorter shear layers and stronger vortices in the wake; and changes to the pressure distribution shown in figure 15. In order to ensure temporal independence, the timestep was again halved to 0.025. From figure 13 it can be seen that this has only marginal variations to the force coefficient histories when compared to the $\Delta tD/U_\infty = 0.05$ case. Isosurfaces of vorticity magnitude for each of the different timesteps are presented in figure 12. Each figure is shown with the same contours values, and it can be seen that the timestep of 0.1 seconds results in much weaker vorticity in the wake.

Note that the forces, pressure distribution, and qualitative flowfield parameters were all close to experimental values when the non-dimensional timestep of 0.1 was used; however, this has been shown to be a fortuitous result since the simulation was temporally underresolved. The underresolution appears to dissipate some of the vorticity in the wake, resulting in longer shear layers, refer to figures 14 and 12. The large variations in the flowfield, apparent from figure 13, resulting from the change in temporal resolution illustrate the importance of ensuring time independence, especially at this Reynolds number where it appears to be relatively sensitive.

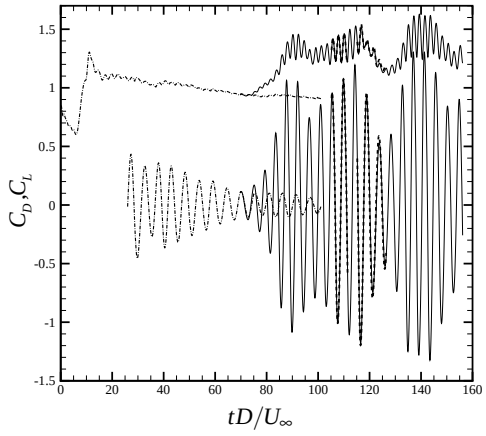

Figure 13: Force coefficient history for 3D URANS case with different timesteps: —·— $\Delta tD/U_\infty = 0.1$; ——— $\Delta tD/U_\infty = 0.05$; - - - - $\Delta tD/U_\infty = 0.025$.

Conclusion

It has been shown that using a three-dimensional URANS model results in only minor improvement over the two-dimensional URANS model for the flow around a circular cylinder at a Reynolds number of 3900. Significant gains can be made by using a LES model, in both bulk quantities and in the wake structure and behaviour. However, these gains are contingent on the LES simulation being fully resolved in the spanwise direction, otherwise the LES model improves only marginally over the three-dimensional URANS model. It is evident at this Reynolds number that data from the URANS is very sensitive to the time step size used in the calculations. Adequate resolution of all temporal scales must be achieved before comparison can be made with experimental data.

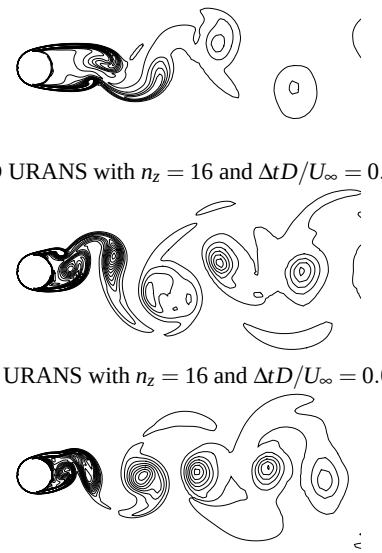

(a) 3D URANS with $n_z = 16$ and $\Delta tD/U_\infty = 0.1$.

(b) 3D URANS with $n_z = 16$ and $\Delta tD/U_\infty = 0.05$.

(c) 3D URANS with $n_z = 16$ and $\Delta tD/U_\infty = 0.025$.

Figure 14: Contours of vorticity magnitude at $Re = 3900$. There are 16 contour levels between 0.5 and 10.

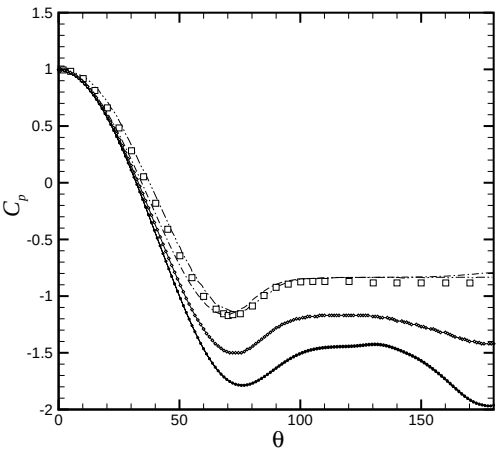

Figure 15: Comparison of the distribution of pressure coefficient around the cylinder: —··— [12] at $Re = 3000$; □ Norberg in [8] at $Re = 4020$; —●— 2*D* URANS; —◇— 3*D* URANS at $\Delta tD/U_\infty = 0.05$; —·— 3*D* URANS at $\Delta tD/U_\infty = 0.1$.

References

[1] Beaudan, P. and Moin, P. *Numerical Experiments on the Flow Past a Circular Cylinder at Sub-critical Reynolds Numbers*, Dept Mech Eng, Stanford Uni, Report No. TF-62, 1994.

[2] Breuer, M., Large eddy simulation of the subcritical flow past a circular cylinder: numerical and modelling aspects, *Int. J. Num. Meth. Fluids*, **28**, 1998, 1281–1302.

[3] Cardell, G.S., Flow past a circular cylinder with a permeable splitter plate, *Ph.D. Thesis*, Cal. Tech., 1993, reported in [2].

[4] Fluent Inc., *Fluent 6.3 User's Guide*, Fluent Inc., Lebanon, 2003.

[5] Franke, R., Rodi,W., and Schönung, B., Numerical calculation of laminar vortex shedding flow past cylinders, *J. Wind Eng. & Ind. Aero.*, **35**, 1990, 237–257.

[6] Ham, F. and Iaccarino, G., Energy conservation in collocated discretization schemes on unstructured meshes, *CTR Annual Research Briefs*, 2004, 3–14.

[7] Jordan, S.A. and Ragab, S.A., A large-eddy simulation of the near wake of a circular cylinder, *J. Fluids Eng*, **120**, 1998, 243–252.

[8] Kravchenko, A.G., and Moin, P., Numerical studies of flow over a circular cylinder at $\mathrm{Re}_D = 3900$, *Phys. Fluids*, **12**, 2000, 403–417.

[9] Lourenco, L.M. and Shih, C., Characteristics of the plane turbulent near wake of a circular cylinder. A particle image velocimetry study, reported in [8].

[10] Mahesh, K., Constantinescu, G., Moin, P. A numerical method for large-eddy simulation in complex geometries, *J. Comp. Phys.*, **197**, 2004, 215–240.

[11] Mittal, R. and Balachandar, S. Effect of three-dimensionality on the lift and drag of nominally two-dimensional cylinders, *Phys. Fluids*, **7**, 1995, 1841–1865.

[12] Norberg, C. *Effects of Reynolds number and low-intensity free stream turbulence on the flow around a circular cylinder*, Publ. No. 87/2, Chalmers University of Technology, Gothenburg, Sweden, 1987.

[13] Norberg, C., Fluctuating lift on a circular cylinder: review and new measurements, *J. Fluids & Struct.*, **17**, 2003, 57–96.

[14] Ong, L. and Wallace, J., The velocity field of the turbulent very near wake of a circular cylinder, *Exp. Fluids*, **20**, 1996, 441–453.

[15] Prasad, A. and Williamson, C.H.K. The instability of the shear layer separating from a bluff body, *J. Fluid Mech.*, **333**, 1997, 375–402.

[16] Roshko, A. *On the Development of Turbulent Wakes from Vortex Streets*, NACA Report 1191, 1954.

[17] Roshko, A., Experiments on the flow past a circular cylinder at very high Reynolds numbers, *J. Fluid Mech.*, **10**, 1961, 345–356.

[18] Tamura, T., Ohta, I. and Kuwahara, K., On the reliability of two-dimensional simulation for unsteady flows around a cylinder-type structure, in *J. Wind Eng & Ind. Aero.*, **35**, 1990, 275–298.

[19] Wilcox, D.C., *Turbulence Modeling for CFD*, DCW Industries, La Cañada, 1998.

[20] Williamson, C.H.K., Oblique and parallel shedding in the wake of a circular cylinder at low Reynolds numbers, *J. Fluid Mech.*, **206**, 1989, 579–627.

[21] Zhou, Y. and Antonia, R., A study of turbulent vortices in the near wake of a circular cylinder, in *J. Fluid Mech.*, **253**, 1993, 643–661.